UNIVERSITY OF BIRMINGHAM

Meshfree and efficient modelling of swimming cells

Gallagher, Meurig Thomas; Smith, David

[Link to publication on Research at Birmingham portal](#)

Meshfree and efficient modeling of swimming cells

Meurig T. Gallagher[*] and David J. Smith[†]

School of Mathematics, University of Birmingham, Edgbaston, Birmingham B15 2TT, United Kingdom

Locomotion in Stokes flow is an intensively studied problem because it describes important biological phenomena such as the motility of many species' sperm, bacteria, algae, and protozoa. Numerical computations can be challenging, particularly in three dimensions, due to the presence of moving boundaries and complex geometries; methods which combine ease of implementation and computational efficiency are therefore needed. A recently proposed method to discretize the regularized Stokeslet boundary integral equation without the need for a connected mesh is applied to the inertialess locomotion problem in Stokes flow. The mathematical formulation and key aspects of the computational implementation in MATLAB® or GNU Octave are described, followed by numerical experiments with biflagellate algae and multiple uniflagellate sperm swimming between no-slip surfaces, for which both swimming trajectories and flow fields are calculated. These computational experiments required minutes of time on modest hardware; an extensible implementation is provided in a GitHub repository. The nearest-neighbor discretization dramatically improves convergence and robustness, a key challenge in extending the regularized Stokeslet method to complicated three-dimensional biological fluid problems.

I. INTRODUCTION

Inertialess locomotion in Stokes flow describes the motility of many types of sperm, bacteria, algae, and protozoa. This topic has received extensive attention from mathematical modelers, starting with the classic work of Taylor [1] and continuing to the present day [2–4]. From the early work into the swimming of sea-urchin spermatozoa [5] to investigations into the orientation of biflagellates in shear flows [6], there has been significant interest in modeling biological swimmers. This interest has been extended recently towards understanding and developing novel microswimmers. Topical examples of these involve studies into the microscale flow dynamics of ribbons and sheets [7] and the modeling of self-propelling toroidal swimmers based on the hypotheses of Taylor and Purcell [8], as well as the study of phoretic toroidal swimmers [9]. Such works have the potential to enable the use of targeted drug delivery, among other things, through being able to guide microswimmers through complex biological environments [10], and improve diagnostics and management of male infertility by analysis of imaging data.

Of particular recent interest is the collective behaviors of microswimmers. The differences in these behaviors appear to have significant biological implications, an example of which is the collective swimming of bovine sperm in the presence of viscoelasticity, behavior which is not apparent in a purely viscous fluid [11]. Other species of sperm exhibit collective behaviors which impact both swimming and the ability to effectively fertilize the egg; some species of opossum sperm are often seen swimming as a cooperative pair [12]. In addition to collective behaviors, the effects of interactions

---

[*]m.t.gallagher@bham.ac.uk

[†]d.j.smith@bham.ac.uk

with other particles and/or boundaries have been recently shown to create interesting dynamics [13–16].

While each of the models presented above are in some sense idealized, the ability to further reduce detailed swimmer models to simplified representations provides the opportunity for extracting significant scientific information which may not be accessible otherwise. Such models allow for creation of a coarse-grained representation of a swimmer [4], reducing complex behavior into a set of swimming modes and their associated limit cycles. Detailed fluid dynamic modeling can also allow for calculation of parameters for continuum models [17] and give understanding of hidden aspects of swimmers' characteristics such as energy transport along a flagellum [18] or internal moment generation [19], as well as providing insight into the exact mechanisms for the collective swimming behaviors mentioned above.

Numerical methods are generally required to model finite-amplitude motions, wall effects, and swimmer-swimmer interactions. A range of numerical approaches exist, with perhaps the most extensively studied being those based on singular or regularized singular solutions of the Stokes flow equations, specifically resistive force theory [5], slender body theory [20], boundary integral methods [21], and regularized Stokeslet methods [22–25]. These techniques remove the need to mesh the volume of fluid, requiring only the solution of integral equations formulated on the surface of the swimming body or bodies and lines such as cilia and flagella, reducing both the cost of meshing and remeshing a continually moving domain and the number of degrees of freedom of the resulting linear system. Other techniques can be used to perform computational analysis of swimmers, such as the use of the force coupling method to investigate the dynamics of suspensions of up to 1000 swimmers [26] and the immersed boundary method [27] for understanding the role of fluid elastic stress on flagellar swimming [28].

As reviewed recently [29], regularized Stokeslet methods have the further major advantage of removing the need to evaluate weakly singular surface integrals and enabling slender bodies such as cilia and flagella to be treated as immersed one-dimensional curves. The original, and most widely used, implementation of the method of regularized Stokeslets of Cortez *et al.* [22] has the further advantage of removing the need to generate a true *mesh*, i.e., a description of the surfaces involved in terms of connected surface elements, as is required by boundary element methods. Instead, it is sufficient to generate a set of points approximating the surfaces and lines of the problem geometry. A disadvantage of the original approach is that it requires many more degrees of freedom than boundary integral methods to achieve converged results.

To improve on the computational efficiency of the regularized Stokeslet method while retaining most of its simplicity of implementation, a method was proposed by Smith [29], involving taking a coarser discretization for the unknown traction than that used for numerical quadrature of the kernel, enabled by the use of nearest-neighbor discretization. The method proved significantly more accurate for significantly lower computational cost, potentially enabling more complex and realistic problems to be investigated with given computational resources.

In this article we generalize the nearest-neighbor discretization three-dimensional regularized Stokeslet method to inertialess locomotion, in particular focusing on uniflagellate pushers modeling human sperm and a model biflagellate. In Sec. II we briefly review the mathematical definition of the inertialess free-swimming problem in the boundary integral formulation. In Sec. III we implement the nearest-neighbor discretization of the free-swimming problem with a single swimmer in an unbounded fluid. We then formulate the task of tracking the trajectory of the cell as an initial-value problem. The discretization is then generalized in Sec. IV to incorporate rigid boundaries and multiple swimming cells. In Sec. V we present the results of numerical experiments with uniflagellate and biflagellate swimmers and in Sec. VI we discuss the method and further practical applications. Key aspects of the implementation in MATLAB®/GNU Octave are given, and a GitHub repository is provided with the full code necessary to generate the results in the paper as well as templates for applying the method to novel problems in very-low-Reynolds-number locomotion.

II. FREE-SWIMMING PROBLEM

The dynamics of a Newtonian fluid at very low Reynolds numbers, associated with locomotion of cells, is described by the Stokes flow equations. The dimensionless form of the equations is

$$-\nabla p + \nabla^2 \boldsymbol{u} = 0, \quad \nabla \cdot \boldsymbol{u} = 0, \tag{1}$$

augmented with the no-slip, no-penetration boundary condition $\boldsymbol{u}(\boldsymbol{X}) = \dot{\boldsymbol{X}}$ for boundary points $\boldsymbol{X}$, where the overdot denotes a time derivative. We note here that, for the kinematic-driven problems in the present paper, the viscosity term has been nondimensionalized out of the partial differential equation; for a force-driven problem the viscosity term would appear in the dimensionless group (the sperm number). Initially we will consider a single swimmer in a three-dimensional unbounded fluid which is stationary at infinity. Two classical problems in Stokes flow are the *resistance problem*, which involves calculating the force and moment on a rigid body made to translate and rotate in stationary fluid, and the *mobility problem*, which involves calculating the rigid-body motion due to an imposed force and moment.

The free-swimming problem in Stokes flow is a variant of the mobility problem. Rather than, or perhaps in addition to, the body being driven by imposed forces, it translates and rotates as a result of changing its shape. In this section we will briefly review this problem, which has been solved numerically in many previous studies, and introduce our notation.

As usual for the regularized Stokeslet method, the fluid velocity u_j at location $\boldsymbol{x}$ (suppressing time dependence) is approximated by a surface integral over the surface ∂D of the swimmer,

$$u_i(\boldsymbol{x}) \approx -\frac{1}{8\pi} \iint_{\partial D} S_{ij}^{\epsilon}(\boldsymbol{x}, \boldsymbol{X}) f_j(\boldsymbol{X}) dS_X. \tag{2}$$

The regularization error associated with Eq. (2) has been discussed previously [22] and will not be reviewed here. In this paper we will treat the approximation as exact. The surface of the body will undergo motions that may be described by a model formulated in a body frame, for example, a frame in which the head of the cell does not move. If the body frame coordinates are $\boldsymbol{\xi}$ and the body frame is described by the matrix of basis vectors (equivalently a rotation matrix) $\boldsymbol{B} = (\boldsymbol{b}^{(1)}|\boldsymbol{b}^{(2)}|\boldsymbol{b}^{(3)})$ and origin $\boldsymbol{x}_0$, then the laboratory frame coordinates and velocities are

$$\boldsymbol{x} = \boldsymbol{x}_0 + \boldsymbol{B} \cdot \boldsymbol{\xi}, \tag{3}$$

$$\dot{\boldsymbol{x}} = \dot{\boldsymbol{x}}_0 + \dot{\boldsymbol{B}} \cdot \boldsymbol{\xi} + \boldsymbol{B} \cdot \dot{\boldsymbol{\xi}}. \tag{4}$$

Denoting the rigid-body velocity and angular velocity of the frame by $\boldsymbol{U}$ and $\boldsymbol{\Omega}$, respectively, we then have

$$\boldsymbol{x} = \boldsymbol{x}_0 + \boldsymbol{B} \cdot \boldsymbol{\xi}, \tag{5}$$

$$\dot{\boldsymbol{x}} = \boldsymbol{U} + \boldsymbol{\Omega} \times (\boldsymbol{x} - \boldsymbol{x}_0) + \boldsymbol{B} \cdot \dot{\boldsymbol{\xi}}. \tag{6}$$

Applying the condition $\boldsymbol{u}(\boldsymbol{x}) = \dot{\boldsymbol{x}}$ on ∂D in Eq. (2) yields the regularized Stokeslet boundary integral equation

$$-\frac{1}{8\pi} \iint_{\partial D} S_{ij}^{\epsilon}(\boldsymbol{x}, \boldsymbol{X}) f_j(\boldsymbol{X}) dS_X = \dot{x}_i \quad \text{for all } \boldsymbol{x} \in \partial D, \tag{7}$$

where it is understood that repeated indices (such as j in the above) are summed over and unrepeated indices (such as i in the above) range over $\{1,2,3\}$.

If at time t the body frame origin $\boldsymbol{x}_0$ and orientation $\boldsymbol{B}$ are known and a model is given for the swimmer shape $\boldsymbol{\xi}$ and motion $\dot{\boldsymbol{\xi}}$ in the body frame, then the unknowns of the problem are the surface traction $\boldsymbol{f}(\boldsymbol{X})$ for $\boldsymbol{X} \in \partial D$, the translational velocity $\boldsymbol{U}$, and the angular velocity $\boldsymbol{\Omega}$. The problem is closed by augmenting Eq. (7) with the force and moment balance equations; here we assume that

the inertia and moment of inertia of the swimmer are negligible. The full problem is then given by

$$-U_i - \epsilon_{ijk}\Omega_j(x_k - x_{0k}) - \frac{1}{8\pi}\iint_{\partial D} S_{ij}^\epsilon(\boldsymbol{x},\boldsymbol{X})f_j(\boldsymbol{X})dS_X = B_{ij}\dot{\xi}_j \quad \text{for all } \boldsymbol{x} \in \partial D,$$

$$\iint_{\partial D} f_i(\boldsymbol{X})dS_X = 0, \tag{8}$$

$$\iint_{\partial D} \epsilon_{ikj}X_k f_j(\boldsymbol{X})dS_X = 0,$$

where ϵ_{ijk} is the Levi-Civita symbol.

Numerical discretization of problem (8) will in general involve N vector degrees of freedom for the traction $\boldsymbol{f}$, three unknowns for the components of the translational velocity $\boldsymbol{U}$, and three unknowns for the components of the angular velocity $\boldsymbol{\Omega}$, totaling $3N + 6$ scalar unknowns in total. Through numerical collocation, problem (8) can be formulated as $3N + 6$ linear equations. In the next section we will describe a nearest-neighbor regularized Stokeslet discretization of this problem.

III. NEAREST-NEIGHBOR DISCRETIZATION

A. Single swimmer in an unbounded fluid

The discretization of the regularized Stokeslet method is discussed in detail in [29]; in brief we suggest that a good balance of ease of implementation and numerical efficiency can be achieved by discretizing the integrals via a quadrature rule, with the key modification of using a finer discretization for the rapidly varying regularized Stokeslet and a coarser discretization for the more slowly varying traction. A simple way to achieve this is through nearest-neighbor interpolation of the traction. The resulting method contains the original and extensively used method of Cortez *et al.* [22] as the limiting case in which the discretizations are equal.

Replacing the integrals in problem (8) with numerical quadrature yields the discrete problem

$$-U_i - \epsilon_{ij\ell}\Omega_j(x_k[m] - x_{0k}) - \frac{1}{8\pi}\sum_{q=1}^{Q} S_{ij}^\epsilon(\boldsymbol{x}[m],\boldsymbol{X}[q])f_j(\boldsymbol{X}[q])dS(\boldsymbol{X}[q]) = B_{ij}\dot{\xi}_j[m]$$

$$\text{for } m = 1, \ldots, N,$$

$$\sum_{q=1}^{Q} f_i(\boldsymbol{X}[q])dS(\boldsymbol{X}[q]) = 0, \tag{9}$$

$$\sum_{q=1}^{Q} \epsilon_{ikj}X_k[q]f_j(\boldsymbol{X}[q])dS(\boldsymbol{X}[q]) = 0,$$

where $dS(\boldsymbol{X}[q])$ denotes the quadrature weight associated with the local surface metric. The coarse traction discretization will be denoted by $\{\boldsymbol{x}[1], \ldots, \boldsymbol{x}[N]\}$ and the finer quadrature discretization by $\{\boldsymbol{X}[1], \ldots, \boldsymbol{X}[Q]\}$; the $Q \times N$ nearest-neighbor matrix is then

$$\nu[q,n] = \begin{cases} 1 & \text{for } n = \underset{\hat{n}=1,\ldots,N}{\arg\min} |\boldsymbol{x}[\hat{n}] - \boldsymbol{X}[q]| \\ 0 & \text{otherwise.} \end{cases} \tag{10}$$

A subtlety here concerns the calculation of the nearest-neighbor matrix when dealing with time-evolving geometries and in particular the case when different bodies approach closely. As an example consider the case of a biflagellate swimmer: As the flagellum gets close to the body there is the potential for a quadrature point on the body to have a nearest force point on the flagellum (or vice versa), leading to incorrect calculation of the traction at these points. For rigid bodies this is easily solved by calculating the nearest-neighbor matrix carefully at a single time point, before the

bodies closely approach, and then treating v as constant in time. Alternatively one can calculate a time-evolving v on a body-by-body basis, considering separately (for example) the discretizations of a flagellum, cell body, and any boundaries.

Defining $g_i[n] := -f_i(\boldsymbol{x}[n])$, the nearest-neighbor interpolation of the traction then corresponds to $-f_i(\boldsymbol{X}[q])dS(\boldsymbol{X}[q]) \approx \sum_{n=1}^{N} v[q,n]g_i[n]dS(\boldsymbol{x}[n])$. Applying this interpolation to problem (9) yields

$$
\frac{1}{8\pi} \sum_{n=1}^{N} g_j[n]dS(\boldsymbol{x}[n]) \sum_{q=1}^{Q} S_{ij}^{\epsilon}(\boldsymbol{x}[m],\boldsymbol{X}[q])v[q,n] - U_i - \epsilon_{ijk}\Omega_j(x_k[m] - x_{0k})
$$

$$
= B_{ij}\dot{\xi}_j[m] \quad \text{for } m = 1, \ldots, N,
$$

$$
\sum_{n=1}^{N} g_j[n]dS(\boldsymbol{x}[n]) \sum_{q=1}^{Q} \delta_{ij}v[q,n] = 0,
$$

$$
\sum_{n=1}^{N} g_j[n]dS(\boldsymbol{x}[n]) \sum_{q=1}^{Q} \epsilon_{ikj}X_k[q]v[q,n] = 0. \tag{11}
$$

Computationally, problem (11) corresponds to $3N + 3 + 3$ linear equations in $3N + 3 + 3$ scalar unknowns ($F_j[n] := g_j[n]dS(\boldsymbol{x}[n])$ for $n = 1, \ldots, N$, followed by U_j and Ω_j). These equations can be expressed in block form as

$$
\begin{pmatrix}
A_{11}^S & A_{12}^S & A_{13}^S & A_1^U & A_1^\Omega \\
A_{21}^S & A_{22}^S & A_{23}^S & A_2^U & A_2^\Omega \\
A_{31}^S & A_{32}^S & A_{33}^S & A_3^U & A_3^\Omega \\
A_1^F & A_2^F & A_3^F & & \\
A_1^M & A_2^M & A_3^M & &
\end{pmatrix}
\begin{pmatrix}
F_1[1] \\ \vdots \\ F_1[N] \\ F_2[1] \\ \vdots \\ F_2[N] \\ F_3[1] \\ \vdots \\ F_3[N] \\ U \\ \Omega
\end{pmatrix}
=
\begin{pmatrix}
B_{1j}\dot{\xi}_j[1] \\ \vdots \\ B_{1j}\dot{\xi}_j[N] \\ B_{2j}\dot{\xi}_j[1] \\ \vdots \\ B_{2j}\dot{\xi}_j[N] \\ B_{3j}\dot{\xi}_j[1] \\ \vdots \\ B_{3j}\dot{\xi}_j[N] \\ \mathbf{0} \\ \mathbf{0}
\end{pmatrix}, \tag{12}
$$

where the blocks have entries given by

$$
A_{ij}^S\{m,n\} = \frac{1}{8\pi} \sum_{q=1}^{Q} S_{ij}(\boldsymbol{x}[m],\boldsymbol{X}[q])v[q,n] \quad \text{for } m,n = 1, \ldots, N,
$$

$$
A_i^U\{m,j\} = -\delta_{ij} \quad \text{for } m = 1, \ldots, N,
$$

$$
A_i^\Omega\{m,j\} = -\epsilon_{ijk}(x_k[m] - x_{0k}) \quad \text{for } m = 1, \ldots, N,
$$

$$
A_j^F\{i,n\} = \delta_{ij} \sum_{q=1}^{Q} v[q,n] \quad \text{for } n = 1, \ldots, N,
$$

$$
A_j^M\{i,n\} = \epsilon_{ikj}X_k \sum_{q=1}^{Q} v[q,n] \quad \text{for } n = 1, \ldots, N
$$

(13)

and the velocity $\boldsymbol{U}$ and angular velocity $\boldsymbol{\Omega}$ are expressed as 3×1 column vectors.

B. Computing swimmer trajectories via an initial-value problem

The position and orientation of a swimmer can be expressed as a position vector and a frame of basis vectors $\boldsymbol{b}^{(j)}$. Given $\boldsymbol{b}^{(1)}$ and $\boldsymbol{b}^{(2)}$, we then have $\boldsymbol{b}^{(3)} = \boldsymbol{b}^{(1)} \times \boldsymbol{b}^{(2)}$, so it is sufficient to formulate the problem in terms of two basis vectors only or six scalar degrees of freedom. Of course, this formulation still contains redundant information; three Euler angles constrain precisely the body frame, however the basis vector approach is very straightforward to implement.

Noting that

$$\dot{\boldsymbol{x}}_0 = \boldsymbol{U}(\boldsymbol{x}_0, \boldsymbol{b}^{(1)}, \boldsymbol{b}^{(2)}, t), \quad \dot{\boldsymbol{b}}^{(j)} = \boldsymbol{\Omega}(\boldsymbol{x}_0, \boldsymbol{b}^{(1)}, \boldsymbol{b}^{(2)}, t) \times \boldsymbol{b}^{(j)}, \quad j = 1, 2, \tag{14}$$

we may then formulate the calculation of trajectories as a system of nine ordinary differential equations, where evaluation of the functions $\boldsymbol{U}(\boldsymbol{x}_0, \boldsymbol{b}^{(1)}, \boldsymbol{b}^{(2)}, t)$ and $\boldsymbol{\Omega}(\boldsymbol{x}_0, \boldsymbol{b}^{(1)}, \boldsymbol{b}^{(2)}, t)$ involves solving the swimming problem (8), for example, via the discretization (11). The outer problem (14) can be solved using built-in functions such as ode45 in MATLAB® or lsode in GNU Octave.

For practical purposes, when using a built-in initial-value problem solver such as ode45, the tractions $f_i(\boldsymbol{X})$, required to compute the rate of energy dissipation and the flow field, may not be automatically available. To record this information, we may introduce the variable $H_i(\boldsymbol{X}, t)$, defined by

$$\dot{H}_i(\boldsymbol{x}, t) = f_i(\boldsymbol{x}, t), \quad \boldsymbol{x} \in \partial D \quad H_i(\boldsymbol{x}, 0) = 0. \tag{15}$$

Augmenting the swimming problem (14) with Eqs. (15) then yields an approximation to the force distribution available external to ode45 by numerically differentiating $H_i(\boldsymbol{x}, t)$ with respect to time.

IV. GENERALIZATION: BOUNDARIES AND MULTIPLE SWIMMERS

A. Boundaries and fixed obstacles

Mammalian sperm usually migrate and fertilize within a thin film of viscous fluid between opposed surfaces and are typically imaged between a microscope slide and coverslip. Indeed, the major effect of boundaries on microswimmer flow fields has long been recognized [30]. Therefore, it is important to take boundary effects into account in fluid dynamic simulations. The Blakelet and its regularized counterpart found by Ainley et al. [31] (see also work by Cortez) is an elegant and efficient way to model a single infinite plane boundary; certain other geometrically simple situations possess similar fundamental solutions. However, it is important for full generality to take into account a more complex boundary, and perhaps also fixed obstacles, present in the flow.

Representing the boundary by B, the swimming problem becomes

$$-U_i - \epsilon_{ijk}\Omega_j(x_k - x_{0k}) - \frac{1}{8\pi}\iint_{\partial D \cup B} S_{ij}^{\epsilon}(\boldsymbol{x}, \boldsymbol{X})f_j(\boldsymbol{X})dS_X = B_{ij}\dot{\xi}_j \quad \text{for all } \boldsymbol{x} \in \partial D,$$

$$-\frac{1}{8\pi}\iint_{\partial D \cup B} S_{ij}^{\epsilon}(\boldsymbol{x}, \boldsymbol{X})f_j(\boldsymbol{X})dS_X = \dot{x}_i \quad \text{for all } \boldsymbol{x} \in B,$$

$$\iint_{\partial D} f_i(\boldsymbol{X})dS_X = 0,$$

$$\iint_{\partial D} \epsilon_{ijk}X_j f_k(\boldsymbol{X})dS_X = 0. \tag{16}$$

Numerically, we may represent the swimmer by the force points $\{\boldsymbol{x}[1], \ldots, \boldsymbol{x}[N_s]\}$ and quadrature points $\{\boldsymbol{X}[1], \ldots, \boldsymbol{X}[Q_s]\}$; the boundary is then discretized by the force points $\{\boldsymbol{x}[N_s + 1], \ldots, \boldsymbol{x}[N_s + N_b]\}$ and quadrature points $\{\boldsymbol{X}[Q_s + 1], \ldots, \boldsymbol{X}[Q_s + Q_b]\}$. Nearest-neighbor

discretization then leads to a system of the form

$$
\begin{pmatrix}
A_{11}^S & A_{12}^S & A_{13}^S & A_1^U & A_1^\Omega \\
A_{21}^S & A_{22}^S & A_{23}^S & A_2^U & A_2^\Omega \\
A_{31}^S & A_{32}^S & A_{33}^S & A_3^U & A_3^\Omega \\
A_1^F & A_2^F & A_3^F & & \\
A_1^M & A_2^M & A_3^M & &
\end{pmatrix}
\begin{pmatrix}
F_1 \\ F_2 \\ F_3 \\ U \\ \Omega
\end{pmatrix}
=
\begin{pmatrix}
V_1 \\ V_2 \\ V_3 \\ \mathbf{0} \\ \mathbf{0}
\end{pmatrix}.
\tag{17}
$$

The blocks have entries given by

$$
A_{ij}^S\{m,n\} = \frac{1}{8\pi}\sum_{q=1}^Q S_{ij}(\boldsymbol{x}[m],\boldsymbol{X}[q])v[q,n] \quad \text{for } m,n = 1,\ldots,N,
$$

$$
A_i^U\{m,j\} = \begin{cases} -\delta_{ij} & \text{for } m = 1,\ldots,N_s \\ 0 & \text{for } m = N_s + 1,\ldots,N_s + N_b, \end{cases}
$$

$$
A_i^\Omega\{m,j\} = \begin{cases} -\epsilon_{ijk}(x_k[m] - x_{0k}) & \text{for } m = 1,\ldots,N_s \\ 0 & \text{for } m = N_s + 1,\ldots,N_s + N_b, \end{cases}
\tag{18}
$$

$$
A_j^F\{i,n\} = \begin{cases} \delta_{ij}\sum_{q=1}^Q v[q,n] & \text{for } n = 1,\ldots,N_s \\ 0 & \text{for } n = N_s + 1,\ldots,N_s + N_b, \end{cases}
$$

$$
A_j^M\{i,n\} = \begin{cases} \epsilon_{ikj}X_k\sum_{q=1}^Q v[q,n] & \text{for } n = 1,\ldots,N_s \\ 0 & \text{for } n = N_s + 1,\ldots,N_s + N_b, \end{cases}
$$

where the total number of force unknowns is $N = N_s + N_b$, the symbols F_j denote $(N_s + N_b) \times 1$ vectors of scalar unknowns $F_j[1],\ldots,F_j[N_s + N_b]$, and the right-hand sides are given by

$$
V_i[n] = \begin{cases} B_{ij}\dot{\xi}_j[n] & \text{for } n = 1,\ldots,N_s \\ 0 & \text{for } n = N_s + 1,\ldots,N_s + N_b. \end{cases}
\tag{19}
$$

B. Multiple swimmers

The last situation we will consider is where there are multiple swimmers, which are not necessarily discretized by equal-size sets, as well as a boundary. The numerical discretization is somewhat more complicated and so we modify our notation in an attempt to make the implementation more interpretable. Suppose that we now have N_{sw} swimmers, described by collocation points with ith components $x_i^{(1)}[\cdot],\ldots,x_i^{(N_{sw})}[\cdot]$, their translational and angular velocities being denoted by $U_i^{(1)},\ldots,U_i^{(N_{sw})}$ and $\Omega_i^{(1)},\ldots,\Omega_i^{(N_{sw})}$, respectively; the boundary points will be denoted by the array $x_i^{(b)}[\cdot]$. The discretization will follow the ordering convention

$$
\mathsf{x} = (\mathsf{x}_1\{\cdot\},\ \mathsf{x}_2\{\cdot\},\ \mathsf{x}_3\{\cdot\})^T \quad \text{with } \mathsf{x}_i\{\cdot\} = \left(x_i^{(1)}[\cdot],\ \ldots,\ x_i^{(N_{sw})}[\cdot],\ x_i^{(b)}[\cdot]\right)^T,
\tag{20}
$$

which is inherited by the right-hand-side velocities and the force discretization. If the number of force points associated with swimmer r is $N_s(r)$ and the number of force points associated with the boundary is N_b, then the number of vector force unknowns is $N_f = \sum_{r=1}^{N_{sw}} N_s(r) + N_b$. The size of x is then $3N_f$ and the total number of scalar degrees of freedom in the system is $3N_f + 6N_{sw}$. We will define the index $\iota(r)$ to be the location of the rth swimmer in the x_i vector, with $\iota(1) = 1$ and $\iota(r) = \sum_{\gamma=1}^{r-1} N_s(\gamma)$ for $1 < r \leqslant N_{sw}$.

The quadrature points may be denoted by $X[1], \ldots, X[Q]$ as previously; the Stokeslet matrix is then constructed as

$$A^S_{ij}\{\alpha,\beta\} = \frac{1}{8\pi} \sum_{q=1}^{Q} S_{ij}(\mathbf{x}_i[\alpha], X[q])v[q,\beta] \quad \text{for } \alpha,\beta = 1, \ldots, N_f. \tag{21}$$

To construct the remaining blocks, we introduce the notation $\mathbf{1}^{(n)}$ to be the column vector of length n with every entry equal to 1 and $\mathbf{0}^{(m \times n)}$ to be the $m \times n$ matrix of zeros. We also define the $N_f \times N_{sw}$ matrices

$$\tilde{x}_i\{\cdot,\cdot\} = \begin{pmatrix} x_i^{(1)}[\cdot] - x_{0i}^{(1)} & & & \\ & \ddots & & \\ & & x_i^{(N_{sw})}[\cdot] - x_{0i}^{(N_{sw})} \\ & \mathbf{0}^{(N_b \times N_{sw})} & \end{pmatrix}. \tag{22}$$

Then

$$A^U = I_3 \otimes \begin{pmatrix} -\mathbf{1}^{[N_s(1)]} & & \\ & \ddots & \\ & & -\mathbf{1}^{[N_s(N_{sw})]} \\ & \mathbf{0}^{(N_b \times N_{sw})} & \end{pmatrix}, \quad A^\Omega = \begin{pmatrix} & -\tilde{x}_3\{\cdot,\cdot\} & \tilde{x}_2\{\cdot,\cdot\} \\ \tilde{x}_3\{\cdot,\cdot\} & & -\tilde{x}_1\{\cdot,\cdot\} \\ -\tilde{x}_2\{\cdot,\cdot\} & \tilde{x}_1\{\cdot,\cdot\} & \end{pmatrix}, \tag{23}$$

with $\otimes$ denoting the Kronecker product.

Recalling that $v[\cdot,\cdot]$ denotes the nearest-neighbor matrix, we define the $N_s(r) \times 1$ column vectors

$$\lambda^{(r)}[\cdot] = \sum_{q=1}^{Q} v[q, \iota(r) : \iota(r+1) - 1], \quad \chi_j^{(r)}[\cdot] = \sum_{q=1}^{Q} X_j(q)v[q, \iota(r) : \iota(r+1) - 1] \tag{24}$$

and the $N_{sw} \times N_f$ matrices

$$\tilde{\chi}_j\{\cdot,\cdot\} = \begin{pmatrix} \chi_j^{(1)T}[\cdot] & & & \\ & \ddots & & \mathbf{0}^{(N_{sw} \times N_b)} \\ & & \chi_j^{(N_{sw})T}[\cdot] & \end{pmatrix}. \tag{25}$$

Then the $3N_{sw} \times 3N_f$ blocks A^F and A^M are

$$A^F = I_3 \otimes \begin{pmatrix} \lambda^{(1)T}[\cdot] & & & \\ & \ddots & & \mathbf{0}^{(N_{sw} \times N_b)} \\ & & \lambda^{(N_{sw})T}[\cdot] & \end{pmatrix},$$

$$A^M = \begin{pmatrix} & -\tilde{\chi}_3 & \tilde{\chi}_2 \\ \tilde{\chi}_3 & & -\tilde{\chi}_1 \\ -\tilde{\chi}_2 & \tilde{\chi}_1 & \end{pmatrix}. \tag{26}$$

Finally, denoting the orientation matrix of the rth swimmer by $B_{ij}^{(r)}$ and its body frame waveform as $\xi_j^{(r)}$, the terms of the right-hand side take the form

$$V_i = \left(V_i^{(1)}[\cdot], \quad \ldots, \quad V_i^{(N_{sw})}[\cdot], \quad \mathbf{0}^{(N_{sw} \times 1)} \right)^T, \tag{27}$$

where

$$V_i^{(r)}[n] = B_{ij}^{(r)} \dot{\xi}_j^{(r)}[n]. \tag{28}$$

Now that we have defined A_{ij}^S, A^U, A^Ω, A^F, A^M, and V_i, the $3(N_f + 2) \times 3(N_f + 2)$ linear system is of the form given by Eq. (17).

V. RESULTS AND ANALYSIS

We now turn our attention to the application of this method to two model problems: (i) a single biflagellate swimming in an infinite fluid and (ii) multiple sperm cells swimming between two boundaries. The implementation for both these model problems is provided in the associated GitHub repository. After presenting the results for these swimming problems we will discuss the convergence of the method for the two types of swimmer provided and compare with the results obtained through the classic Nyström discretization (when the force and quadrature discretizations are the same).

A. Biflagellate in an infinite fluid

We will first apply the algorithm in Sec. III A to model a biflagellate, superficially similar to various marine algae, swimming in an unbounded fluid. We model the beat pattern of the cell [Fig. 1(a)] following Sartori *et al.* [32], writing the flagellar tangent angle ψ in the form

$$\psi(s,t) = \psi_0(s) - \psi_1(s) \cos [t + \phi(s)], \tag{29}$$

where s and t are dimensionless arc lengths along the flagellum and time, respectively. We find that choosing

$$\psi_0(s) = -2.5s, \quad \psi_1 = 0.7 + 0.15 \sin(2\pi s), \quad \phi(s) = -2\pi s, \quad 0 \leqslant s \leqslant 1, \tag{30}$$

provides a sufficiently representative test case for the computational algorithm. Of course a more realistic beat for a genuine biflagellate species such as *Chlamydomonas reinhardtii* could be appended as required.

The two flagella are synchronized; for the force discretization, 40 points are used to discretize each flagellum and 96 points are used for the cell body, totaling 176 vector degrees of freedom (Fig. 1). For the quadrature discretization, 400 points are used for each flagellum and 600 points for the cell body, giving a total of 1400 quadrature points [Fig. 1(b)]. The regularization parameter is chosen as $\epsilon = 0.25/20$ to represent the radius of the flagellum (scaled with flagellar length).

Results showing the displacement of the swimming cell are shown in Fig. 1(c) and the flow field at three points of the beat in Figs. 1(d)–1(f). The latter calculation can be carried out in a postprocessing step from the computed swimmer position, orientation, and force distribution. To further visualize the flow we have included in Figs. 1(g) and 1(h) a selection of streamlines plotted over the fluid velocity. While the figures show a two-dimensional projection, the computation is fully three dimensional and the instantaneous flow field on any (finite) subset of $\mathbb{R}^3$ can be computed. The computation and creation of Fig. 1 required 33.4 s on a desktop computer [2017 Lenovo Thinkstation P710; Intel(R) Xeon(TM) E5-2646 CPU @ 2.40 GHz; 128 GB 2400 MHz RDIMM RAM].

B. Sperm between two opposed surfaces

We now turn our attention to the more general problem of Sec. IV B involving multiple swimming cells and boundaries. The computational domain contains two no-slip square surfaces with sides of length $3L$, separated by a distance $0.4L$, where L is the flagellar length (for human sperm typically $L \approx 45$ μm). The swimmer heads are ellipsoids with axes of length $0.044L$, $0.036L$, and $0.022L$. The flagellar movement is based on the classic planar activated beat of Dresdner and Katz [33]; the sperm head (cell body) is a scalene ellipsoid. Figures 2(a) and 2(b) show the beat pattern via the force and quadrature discretizations, respectively. The force discretization consists of 136 points per cell and 480 points for the boundary, totaling 3480 scalar degrees of freedom (DOF) for a simulation with five cells. The quadrature discretization consists of 700 points per swimmer and 1920 points for the boundary, totaling 5420 quadrature points. The regularization parameter is chosen as $\epsilon = 0.25/45$ to represent the radius of the flagellum (scaled with flagellar length).
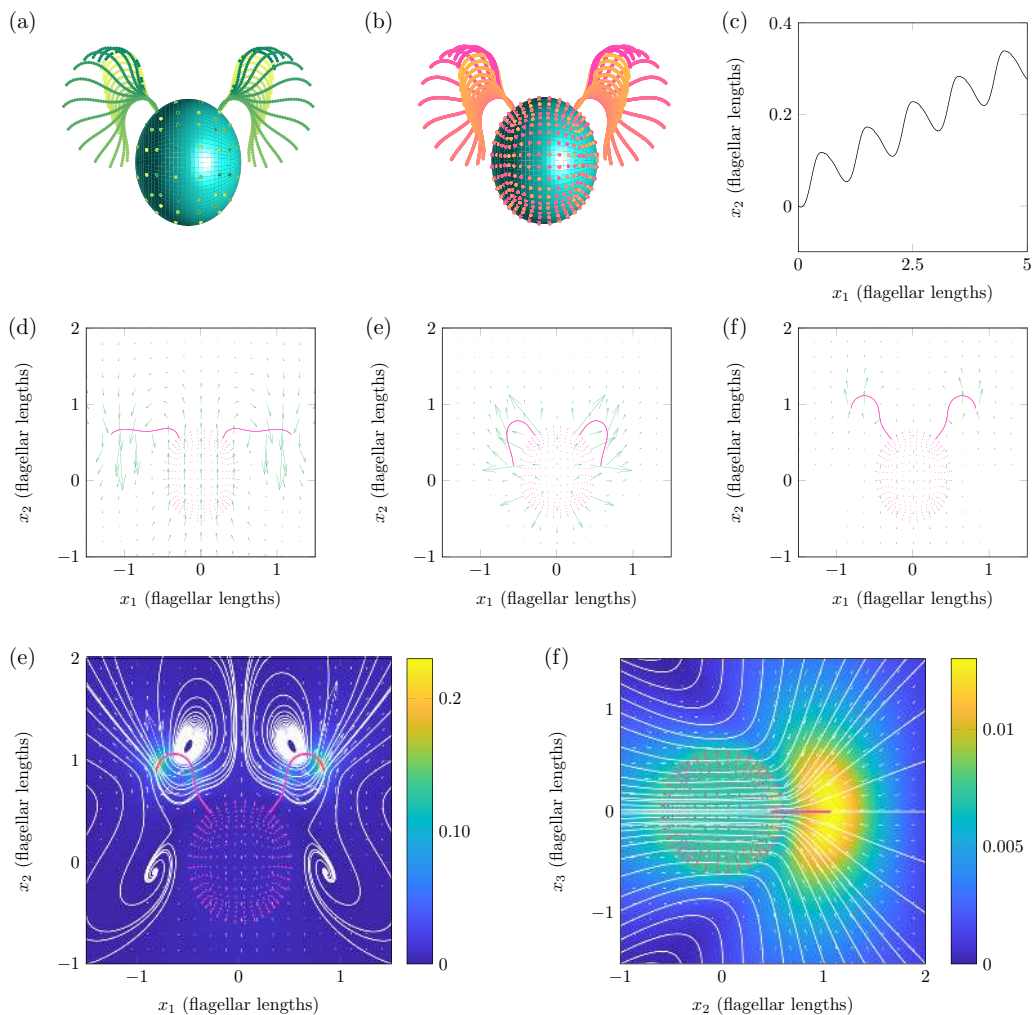
FIG. 1. Computational results for a free-swimming model biflagellate in an unbounded fluid, implemented with the script `GenerateSwimmingFigureChlamy.m`. Model biflagellate show the beat pattern, visualized via (a) force discretization and (b) quadrature discretization. (c) The x_2 coordinate of the free-swimming cell over five beat cycles, where positive x_2 is the overall swimming direction. The computed flow fields are shown at (d) $t = 2\pi/3$, (e) $t = 4\pi/3$, and (f) $t = 2\pi$ (three points during the beat cycle). The computed velocity profile with streamlines is shown at $t = 0$ for cross sections of the (g) (x_1, x_2) and (h) (x_2, x_3) planes.

The computation shown in Fig. 2 involves tracking five cells, each with slightly perturbed beat cycle and head morphology parameters, swimming midway between the no-slip boundaries described above [visualized in Fig. 2(c)], for five beat cycles. Figure 2(d) shows the cell trajectories and Figs. 2(d) and 2(e) show the cell positions, orientations, and surrounding flow fields at two distinct time points. To further visualize the flow we have included in Figs. 2(g) and 2(h) a selection of streamlines plotted over the fluid velocity. The calculated dimensionful swimmer velocity is approximately equal to 43 μm s^{-1}, which is comparable to the results of Smith *et al.* [34], who report a numerical calculation of the speed of a sperm with the same waveform, swimming at a distance 0.2 flagellar lengths from a surface, as approximately equal to 42 μm s^{-1}. While the computation was more intensive than that described in the preceding section, it was still easily within reach of the same computer, requiring 127 s of wall time.
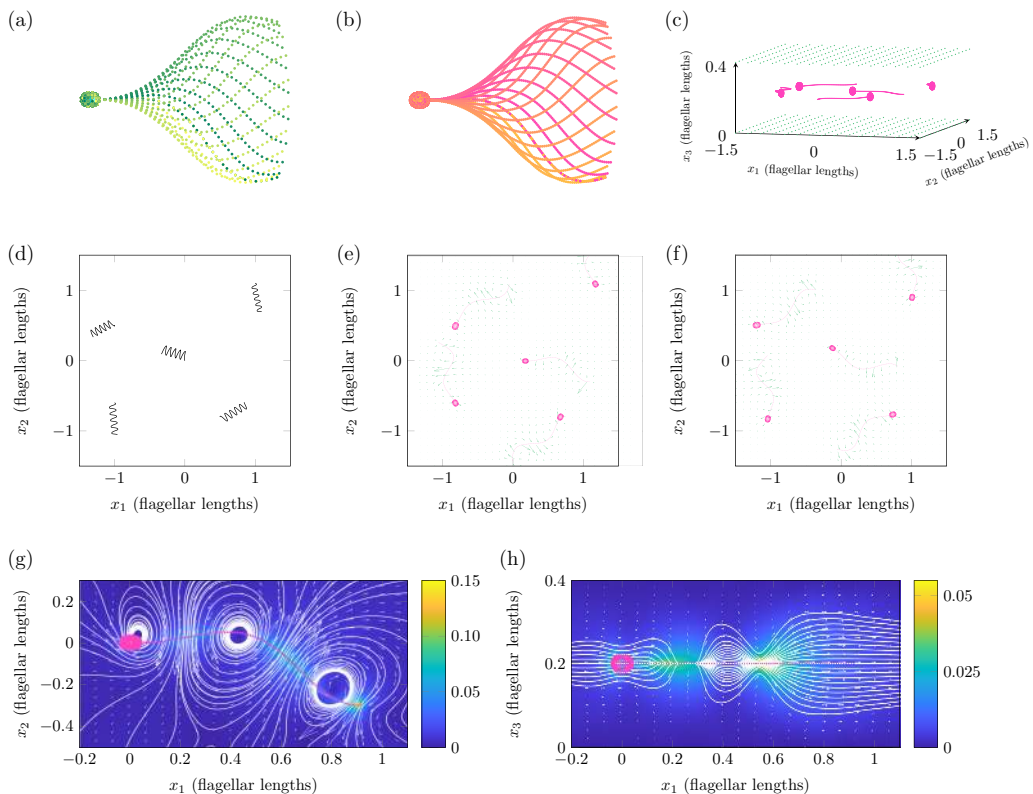
FIG. 2. Computational results for a group of free-swimming model sperm swimming midway between two opposed no-slip surfaces separated by 0.4 flagellar lengths, implemented with the script `GenerateSwimmingFigureSperm.m`. Model sperm show the beat pattern of Dresdner and Katz [33], visualized via (a) force discretization and (b) quadrature discretization. (c) Visualization of sperm placed between the discretized boundaries (note that the sperm heads appear rounder than they actually are due to the aspect ratio chosen for plotting). (d) Trajectories of free-swimming cells over five beat cycles. The computed cell positions (with five randomly perturbed beat cycles and head dimensions) and flow fields are shown at (e) $t = 0$ and (f) $t = 2.5$ cycles. The computed velocity profile with streamlines of a single sperm is shown at $t = 0$ for cross sections of the (g) (x_1, x_2) and (h) (x_1, x_3) planes.

C. Convergence of the method with discretization refinement

A practical refinement heuristic for assessing the convergence (with increased discretization) of the nearest-neighbor method is given by Smith [29]. For testing the convergence of the present swimming problems we define the maximum discretization spacings from [29] as

$$h_f = \max_{m=1,\ldots,N} \min_{\substack{n=1,\ldots,N \\ n \neq m}} |\boldsymbol{x}[m] - \boldsymbol{x}[n]|, \quad h_q = \max_{p=1,\ldots,Q} \min_{\substack{q=1,\ldots,Q \\ q \neq p}} |\boldsymbol{X}[p] - \boldsymbol{X}[q]|. \quad (31)$$

In the present work we note that we may have different discretizations for each swimmer and indeed for each component of a single swimmer (the head and flagellum may be discretized differently, for example). To this end we apply the existing convergence heuristic in stages as outlined in Table I (see also [35]). To measure the convergence we compare the straight line distance traveled over one full beat of the swimmer's flagellum. In contrast to the classical (Nyström) discretization [22], there is no tight coupling between the regularization parameter ϵ and the discretization length scales [29]. As a

TABLE I. Heuristic for analyzing the convergence of the results.

1. Generate an initial force and quadrature discretization for the swimmer head h_f^H and h_q^H.
2. Assess convergence by the heuristic in [29] through varying the flagellar discretizations h_f^F and h_q^F.
3. Generate a more refined head quadrature discretization by halving h_q^H and repeat step 2.
4. Generate a more refined head force discretization by halving h_f^H and repeat step 2.
5. Repeat steps 3 and 4 until a suitable level of convergence is reached.

consequence of this we allow the choice of regularization parameter ϵ to be guided by the geometry of the swimmer (chosen here to be related to the dimensions of the flagellum).

We have analyzed the convergence of the results for the following cases: a single swimming biflagellate (as described in Sec. V A), a single swimming sperm (as in Sec. V B) with no boundary, and a single swimming sperm with boundary. We also assess the effect of the boundary through fixing the sperm discretization and applying the heuristic of Table I to the boundary discretizations and through fixing the sperm and boundary discretizations and increasing the boundary length. The effects of refining the flagellum discretizations in the biflagellate and single sperm models are shown in Tables II and III, with the full convergence results provided in the Supplemental Material [35]. Here we have used the straight line distance traveled by the swimmer as the objective for convergence, and it is clear from Tables II and III, together with the associated tables in the Supplemental Material, that the method is well converged for each swimmer, both in the presence of boundaries and not.

TABLE II. Our nearest-neighbor convergence results: straight line distance traveled by a single biflagellate swimmer, as described in Sec. V A, after one complete flagellar beat cycle. Here the discretization for the cell head is fixed with $N^H = 96$ and $Q^H = 600$ force and quadrature points, respectively. The number of points discretizing the flagellum have been chosen following the convergence algorithm in Table I, with the regularization parameter $\epsilon = 0.25/20$ being the ratio between flagellar radius and length. When $N^F > Q^F$ a singular linear system is formed; this is denoted by the entry NaN (not a number). (a) Distance traveled by the swimmer. Also shown is the percentage change in this distance when halving (b) h_f^F and (c) h_q^F.

(a) Distance traveled in multiples of (flagellar length) $\times 10^{-2}$

				Q^H	600	600	600	600
				h_q^H	0.1137	0.1137	0.1137	0.1137
				Q^F	100	200	400	800
DOF	N^H	h_f^H	N^F	h_f^F $\diagdown$ h_q^F	0.09767	0.04859	0.02424	0.01210
528	96	0.2272	40	0.2479	5.521	5.521	5.526	5.527
768	96	0.2272	80	0.1224	5.503	5.501	5.498	5.498
1248	96	0.2272	160	0.06082	NaN	5.504	5.503	5.502
2208	96	0.2272	320	0.03032	NaN	NaN	5.487	5.432

(b) Percentage change in distance traveled when halving h_f^F

h_f^F $\diagdown$ h_q^F	0.09767	0.04859	0.02424	0.01210
0.1224	0.32%	0.37%	0.49%	0.52%
0.06082		0.06%	0.08%	0.08%
0.03032			0.29%	1.28%

(c) Percentage change in distance traveled when halving h_q^F

h_f^F $\diagdown$ h_q^F		0.04859	0.02424	0.01210
0.2479		0.01%	0.08%	0.02%
0.1224		0.03%	0.05%	0.01%
0.06082			0.02%	0.01%
0.03032				1.00%

TABLE III. Our nearest-neighbor convergence results: straight line distance traveled by a single sperm, swimming between two opposed surfaces, as described in Sec. IV B, after one complete flagellar beat cycle. Here the discretization for the cell head is fixed with $N^H = 96$ and $Q^H = 600$ force and quadrature points, respectively. The number of points discretizing the flagellum have been chosen following the convergence algorithm in Table I, with the regularization parameter $\epsilon = 0.25/45$ being the ratio between flagellar radius and length. When $N^F > Q^F$ a singular linear system is formed, this is denoted by the entry NaN (not a number). (a) Distance traveled by the swimmer. Also shown is the percentage change in this distance when halving (b) h_f^F and (c) h_q^F.

(a) Distance traveled in multiples of (flagellar length) $\times 10^{-2}$

					Q^H 600	600	600	600	600
					h_q^H 0.006702	0.006702	0.006702	0.006702	0.006702
					Q^F 100	200	400	800	1600
DOF	N^H	h_f^H	N^F	h_f^F	h_q^F 0.01011	0.005032	0.002510	0.001254	0.0006265
408	96	0.01314	40	0.02564	6.912	6.957	6.992	7.004	7.011
528	96	0.01314	80	0.01267	7.003	6.935	6.939	6.749	6.950
768	96	0.01314	160	0.006297	NaN	6.925	6.924	6.924	6.924
1248	96	0.01314	320	0.003140	NaN	NaN	6.920	6.918	6.919

(b) Percentage change in distance traveled when halving h_f^F

h_f^F \ h_q^F	0.01011	0.005032	0.002510	0.001254	0.0006265
0.01267	1.32%	0.31%	0.75%	3.64%	0.86%
0.006297		0.15%	0.21%	2.59%	0.39%
0.003140			0.05%	0.09%	0.07%

(c) Percentage change in distance traveled when halving h_q^F

h_f^F \ h_q^F	0.005032	0.002510	0.001254	0.0006265
0.02564	0.65%	0.50%	0.18%	0.10%
0.01267	0.97%	0.06%	2.74%	2.98%
0.006297		0.01%	0.01%	0.00%
0.003140			0.04%	0.01%

Increasing the size of the boundaries resulted in a negligible change to the distance traveled by the swimmer. We note here that the head discretization for the sperm case is very fine; this has been chosen to illustrate the convergence results following the heuristic of Smith [29].

For comparison with our method, in Table IV we present the straight line distance traveled by the biflagellate swimmer when the Nyström discretization is used. We can see from the data in the Table IV that the Nyström discretization requires 8538 degrees of freedom ($N^H = 2646$ and $N^F = 100$) to approach within 1% the converged distance of approximately 5.5×10^{-2} flagellar lengths, while the current method is within 1% of the converged distance in the first entry of Table II, with only 528 degrees of freedom ($N^H = 96$ and $N^F = 40$). In Fig. 3 we show the convergence of the swimming distance for both the nearest-neighbor and classic (Nyström) discretizations, where for the former we have chosen the quadrature discretization to be twice as fine as the force. This figure visually emphasizes the convergence results of Tables II and IV from which we see that, for the choice of $\epsilon = 0.25/20$, the Nyström method requires many more degrees of freedom to reach the same levels of convergence. This convergence rate could be improved in the Nyström case by varying ϵ (as discussed in [22]); however, as previously discussed, the nearest-neighbor discretization is much more robust to this parameter.

VI. DISCUSSION

This paper has described an extension of the nearest-neighbor regularized Stokeslet method [29] to enable the simulation of multiple force- and moment-free cells swimming in a bounded domain. Cell trajectory calculations were achieved by casting the task as an initial-value problem; by integrating

TABLE IV. Nyström (classical) regularized Stokeslet convergence results for comparison purposes: straight line distance traveled by a single biflagellate swimmer, as described in Sec. V A, after one complete flagellar beat cycle with the Nyström discretization. The number of points has been chosen following the convergence algorithm in Table I, with the regularization parameter $\epsilon = 0.25/20$ being the ratio between flagellar radius and length. (a) Distance traveled by the swimmer. Also shown is the percentage change in this distance when doubling (b) N^H and (c) N^F.

(a) Distance traveled in multiples of (flagellar length) $\times 10^{-2}$

N^H \ N^F	40	100	200	400
96	6.542	7.148	7.151	7.165
600	5.320	5.794	5.803	5.819
2646	5.105	5.554	5.563	5.578

(b) Percentage change in distance traveled when doubling N^F

N^H \ N^F	100	200	400
96	9.29%	0.05%	0.19%
600	8.91%	0.14%	0.28%
2646	8.79%	0.16%	0.27%

(c) Percentage change in distance traveled when doubling N^H

N^H \ N^F	40	100	200	400
600	18.68%	18.94%	18.86%	18.79%
2646	4.04%	4.15%	4.13%	4.15%

the force at each step it was additionally possible to store the evolving force distribution to enable postcalculation of the velocity field. The method was assessed on two problems of a type which may be of interest in the biological fluid mechanics community: swimming of a biflagellate in an unbounded domain and motility of multiple human sperm between two no-slip surfaces.

Numerical experiments provide evidence that the method is relatively efficient and converges well, requiring minutes to solve the problems described above, without specialist computational hardware, and we note with interest the significantly improved convergence of this method when compared to the classic Nyström discretization. While the construction of the matrices is somewhat tedious, the underlying concept of the method, using coarse and fine discretizations of the boundary integral equations to address the fact that the force distribution varies more slowly than the kernel, should ensure that the method is comprehensible and extensible by nonspecialists. Crucially, no true
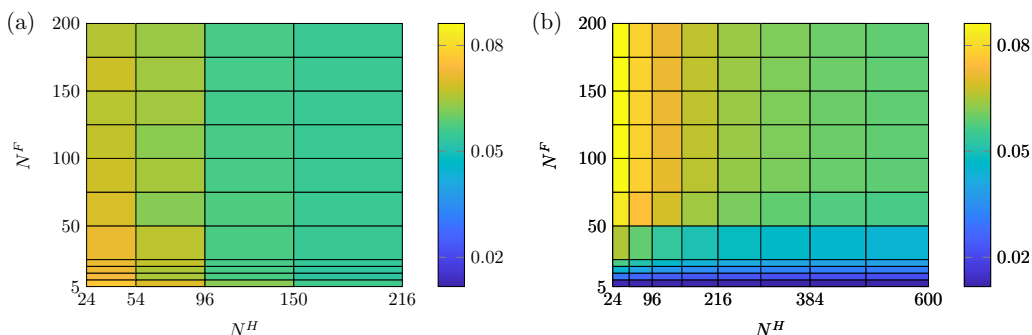

FIG. 3. Visual comparison of how the swimming distance for the biflagellate swimmer converges with (a) the nearest-neighbor and (b) the classic (Nyström) discretizations. The swimming distance is shown with increasing number of points for both the head (N^H) and flagellum (N^F) discretizations. In (a) the quadrature discretization is chosen to be twice as fine as the force discretization.

mesh generation (i.e., with connectivity tables) is required to simulate a new swimmer of interest. We hope that these properties of ease of use, extensibility, and efficiency make the method appealing to potential users, and in support of this aim we provide all MATLAB® code used to generate this report in a repository [36]. Within this repository, a template file `nnSwimmerTemplate.m` is provided which sets out how new swimmers can be added to the existing codebase.

There are many potential extensions for this work spanning the whole field of locomotion at low Reynolds number. The convergence properties of this method mean that it may be valuable for high-throughput analysis of experimental data or (perhaps with adaptations to deal efficiently with long-range interactions) suspensions of relatively large numbers of swimmers. It would be interesting to see if the modification of the method to take into account viscoelastic effects would allow for the collective swimming behavior of sperm seen by Tung *et al.* [11] to be reproduced from an idealized model of swimming. There is potential for this method to be applied to the world of phoretic swimmers to examine the dynamics of many phoretic particles or to the case of swimmers driven by magnetic fields. The computational efficiency of this method can also be exploited through modeling multiple swimmers in complex environments, for example, ciliary flow. While such flows would previously have been simulated and then applied as a background flow to a swimmer, with this efficient method one would be able to model the ciliary beating patterns directly and could allow for a more realistic interaction between swimmers and their environment.

[1] G. I. Taylor, Analysis of the swimming of microscopic organisms, Proc. R. Soc. London Ser. A **209**, 447 (1951).

[2] E. E. Keaveny, S. W. Walker, and M. J. Shelley, Optimization of chiral structures for microscale propulsion, Nano Lett. **13**, 531 (2013).

[3] J. Simons, L. Fauci, and R. Cortez, A fully three-dimensional model of the interaction of driven elastic filaments in a Stokes flow with applications to sperm motility, J. Biomech. **48**, 1639 (2015).

[4] K. Ishimoto, H. Gadêlha, E. A. Gaffney, D. J. Smith, and J. Kirkman-Brown, Coarse-Graining the Fluid Flow around a Human Sperm, Phys. Rev. Lett. **118**, 124501 (2017).

[5] J. Gray and G. J. Hancock, The propulsion of sea-urchin spermatozoa, J. Exp. Biol. **32**, 802 (1955).

[6] S. O'Malley and M. A. Bees, The orientation of swimming biflagellates in shear flows, Bull. Math. Biol. **74**, 232 (2012).

[7] T. D. Montenegro-Johnson, L. Koens, and E. Lauga, Microscale flow dynamics of ribbons and sheets, Soft Matter **13**, 546 (2017).

[8] J. Huang and L. Fauci, Interaction of toroidal swimmers in stokes flow, Phys. Rev. E **95**, 043102 (2017).

[9] L. C. Schmieding, E. Lauga, and T. D. Montenegro-Johnson, Autophoretic flow on a torus, Phys. Rev. Fluids **2**, 034201 (2017).

[10] T. D. Montenegro-Johnson, Microtransformers: Controlled microscale navigation with flexible robots, arXiv:1801.09742v1.

[11] C.-k. Tung, C. Lin, B. Harvey, A. G. Fiore, F. Ardon, M. Wu, and S. S. Suarez, Fluid viscoelasticity promotes collective swimming of sperm, Sci. Rep. **7**, 3152 (2017).

[12] P. Cripe, O. Richfield, and J. Simons, Sperm pairing and measures of efficiency in planar swimming models, Spora A. J. Biomath. **2**, 5 (2016).

[13] J. Simons, S. Olson, R. Cortez, and L. Fauci, The dynamics of sperm detachment from epithelium in a coupled fluid-biochemical model of hyperactivated motility, J. Theor. Biol. **354**, 81 (2014).

[14] E. Lushi, V. Kantsler, and R. E. Goldstein, Scattering of biflagellate microswimmers from surfaces, Phys. Rev. E **96**, 023102 (2017).

[15] H. Shum and J. M. Yeomans, Entrainment and scattering in microswimmer-colloid interactions, Phys. Rev. Fluids **2**, 113101 (2017).

[16] A. Zöttl and J. M. Yeomans, Enhanced bacterial swimming speeds in macromolecular polymer solutions, arXiv:1710.03505.

[17] T. J. Pedley and J. O. Kessler, A new continuum model for suspensions of gyrotactic micro-organisms, J. Fluid Mech. **212**, 155 (1990).

[18] E. A. Gaffney, H. Gadêlha, D. J. Smith, J. R. Blake, and J. C. Kirkman-Brown, Mammalian sperm motility: Observation and theory, Annu. Rev. Fluid Mech. **43**, 501 (2011).

[19] C. J. Brokaw, Bend propagation by a sliding filament model for flagella, J. Exp. Biol. **55**, 289 (1971).

[20] J. J. L. Higdon, A hydrodynamic analysis of flagellar propulsion, J. Fluid Mech. **90**, 685 (1979).

[21] N. Phan-Thien, T. Tran-Cong, and M. Ramia, A boundary-element analysis of flagellar propulsion, J. Fluid Mech. **185**, 533 (1987).

[22] R. Cortez, L. Fauci, and A. Medovikov, The method of regularized Stokeslets in three dimensions: Analysis, validation, and application to helical swimming, Phys. Fluids **17**, 031504 (2005).

[23] E. A. Gillies, R. M. Cannon, R. B. Green, and A. A. Pacey, Hydrodynamic propulsion of human sperm, J. Fluid Mech. **625**, 445 (2009).

[24] V. Shankar and S. D. Olson, Radial basis function (RBF)-based parametric models for closed and open curves within the method of regularized Stokeslets, Int. J. Numer. Meth. Fl. **79**, 269 (2015).

[25] M. W. Rostami and S. D Olson, Kernel-independent fast multipole method within the framework of regularized Stokeslets, J. Fluid. Struct. **67**, 60 (2016).

[26] S. F. Schoeller and E. E. Keaveny, From flagellar undulations to collective motion: Predicting the dynamics of sperm suspensions, J. R. Soc. Interface **15**, 20170834 (2018).

[27] C. S. Peskin, The immersed boundary method, Acta Numer. **11**, 479 (2002).

[28] C. Li, B. Qin, A. Gopinath, P. E. Arratia, B. Thomases, and R. D. Guy, Flagellar swimming in viscoelastic fluids: Role of fluid elastic stress revealed by simulations based on experimental data, J. R. Soc. Interface **14**, 20170289 (2017).

[29] D. J. Smith, A nearest-neighbour discretisation of the regularized Stokeslet boundary integral equation, J. Comput. Phys. **358**, 88 (2018).

[30] N. Liron and J. R. Blake, Existence of viscous eddies near boundaries, J. Fluid Mech. **107**, 109 (1981).

[31] J. Ainley, S. Durkin, R. Embid, P. Boindala, and R. Cortez, The method of images for regularized Stokeslets, J. Comput. Phys. **227**, 4600 (2008).

[32] P. Sartori, V. F. Geyer, A. Scholich, F. Jülicher, and J. Howard, Dynamic curvature regulation accounts for the symmetric and asymmetric beats of *Chlamydomonas* flagella, eLife **5**, e13258 (2016).

[33] R. D. Dresdner and D. F. Katz, Relationships of mammalian sperm motility and morphology to hydrodynamic aspects of cell function, Biol. Reprod. **25**, 920 (1981).

[34] D. J. Smith, E. A. Gaffney, J. R. Blake, and J. C. Kirkman-Brown, Human sperm accumulation near surfaces: A simulation study, J. Fluid Mech. **621**, 289 (2009).

[35] See Supplemental Material at http://link.aps.org/supplemental/10.1103/PhysRevFluids.3.053101 for the complete set of convergence tables for the swimmers provided in this paper.

[36] Available at github.com/djsmithbham/nearestStokesletsSwimmers.